Journal of nanoporous Systems

Original Research Paper

Targeted drug delivery of temozolamide to cancer cells using SBA-16 modified mesoporous nanostructure

Samaneh Soleymani[1, *], Maryam Razavi Mehr[2]

[1]*Department of Chemistry, Faculty of Chemistry, Lorestan University, Khorramabad, Iran*

[2]*Department of Education, Faculty of Teacher Education, Farhangian University, Boroujerd, Iran*

Article history
Received: 7 July 2025
Revised: 28 August 2025
Accepted: 2 September 2025

*Corresponding Author,
Email: soleymani.sa@fs.lu.ac.ir

Abstract: This study presents a design for a controlled drug delivery system using modified SBA-16 mesostructured as carrier and temozolamide as drug. Physicochemical properties to confirm the structure of modified SBA-16 after synthesis were characterized using X-ray diffraction (XRD), Fourier transform infrared spectroscopy (FTIR), scanning electron microscopy (SEM), transmission electron microscopy (TEM) and elemental analysis (EDX). The effect of effective parameters on drug loading including pH, initial drug concentration, nanocarrier amount, temperature and contact time were investigated using response surface methodology (RSM), central combination model (CCD) by design of experiment (DOE) software. Drug release was studied in three simulated body environments at 37°C, including neutral environment with pH=6.8, acidic environment with pH=4.8 and alkaline environment with pH=7.4 at times of 1, 2, 3, 4, 12, 24, 48 and 72 hours. The data obtained from isotherm determination and drug loading kinetic studies showed that the drug loading process followed the Langmuir isotherm with R^2 = 0.9936 and the quasi-kinetic second-order model with R^2 = 0.9953. Also, thermodynamic studies showed that drug loading onto the synthesized nanocarrier is an exothermic and spontaneous process.

Keywords: Drug loading, Drug release, Mesoporous silica nanoparticles, Drug delivery systems, Temozolamide, Experimental design.

Introduction

Glioblastoma is the most common malignant brain tumor in adults. Treatment of tumors, especially glioblastoma, is a challenging issue because the average survival time for patients is less than one year. Temozolamide (Fig 1) is an efficient alkylating agent used in the treatment of brain tumors. The use of temozolamide can increase the survival period from 12.1 months to 14.6 months in patients with high-grade glioma. This 2.5-month increase in survival is a major advance in treatment. Temozolamide has 100% bioavailability with a short half-life, therefore, high doses are necessary. However, high doses cause severe side effects such as melium poisoning, thrombocytopenia, ulceration, nausea, diarrhea, fatigue, and headache, which limit its effectiveness. The use of modern drug delivery systems is a new strategy that can eliminate the side effects of temozolamide and increase its efficacy and reduce toxicity [1-3]. Table 1 shows the physicochemical properties of temozolamide relevant to targeted drug delivery.

New drug delivery system (NDDS) is a term mainly associated with the formulation of new dosage forms that have optimized properties such as smaller particle size, higher permeability parameters and site-selective targeting. NDDSs can be used to enhance the performance of bio therapeutic agents compared to their effect in conventional dosage forms. A new drug delivery system is a novel approach that uses new technologies, innovative ideas and methodologies to deliver active molecules in a safe yet effective concentration to produce the desired drug effect [4]. The new drug delivery system can also maintain the drug concentration in the plasma in a controlled manner to achieve the desired effect for a longer period of time. Therefore, compared to the conventional dosage form, it increases the performance of the drug in terms of safety, efficacy and patient compliance [5]. The process of targeted drug delivery maintains the level of appropriate drug concentrations for a long period of time and reduces many limitations of conventional treatment such as the number of doses used, the initial

concentration of the drug, as well as the side effects caused by the simple release of the drug in an uncertain systemic distribution. Each targeted delivery system includes a drug, a carrier and a targeting ligand, in which the distribution, metabolism and cellular absorption of the drug are determined according to the physicochemical properties and biological behavior of the carrier and ligand. Therefore, the design of the appropriate carrier and ligand increases the efficiency of the drug in the diseased tissue and reduces the toxicity of the drug in other healthy tissues [6]. Drug delivery systems (DDS) are created in order to improve the medicinal and therapeutic properties of drugs used in patients, and often contain the drug in a reservoir. These systems release the drug in a certain amount and in a specific place, thus affecting the pharmacokinetics and distribution of the drug in the body. Nanoparticles are widely used in drug delivery. In recent years, special attention has been paid to nanostructures as drug carriers; Because these structures control and slow down the drug release, protect the drug molecule, particle size smaller than the cell, the ability to cross biological barriers to deliver the drug to the target site, increase the drug's shelf life in the bloodstream, targeted drug delivery and biocompatibility. be considered a very effective drug delivery system; which increase the therapeutic efficiency of the drug. During the last half century, advances in related sciences; Such as polymer science and chemistry, biology as well as mechanical and physics sciences have all been able to influence the variety of nanocarriers and introduce various categories of carriers with unique properties and different efficiency to medical science [7-9].

Among all the existing nanomaterials, several studies have investigated porous silica nanoparticles due to their unique properties, such as large surface area and pore volume, controllable particle size, and good biocompatibility. Mesoporous silica nanoparticles (MSN) have attracted much attention in the last decade due to their unique and tunable physicochemical properties. Among the mesoporous silicon compounds, Santa Barbara amorphous compounds can be mentioned. These compounds were synthesized in 1998 by Zhao et al. at the University of Santa Barbara in California. The compositions of SBAs contain mesopores with a size of 50 to 300 angstroms [10]. The wall material of these compounds is silicate and they have a surface area of about 600-1000 square meters per gram. For the synthesis of this category of mesoporous compounds, the three-part copolymer EO-PO-EO (polyethylene oxide and polypropylene oxide) is used as a structure directing agent and silica precursor as a source of silica in acidic conditions. The synthesized mesoporous silica has a regular porous structure and is quite effective in adsorbing pharmaceuticals or other organic compounds [11]. Due to having large pores, it provides enough space for large drug molecules and absorption of more than 80% of the initial concentration. In general, mesoporosity is one of the important factors for better absorption of medicinal substances on silica or related adsorbents. Among the SBA compounds, SBA-16 with Im3m symmetry and cubic structure is synthesized using poly (ethylene oxide)-poly (propylene oxide)-poly(ethylene oxide) triblock Pluronic copolymer F127 with a pore diameter above 5 nm. Also, SBA-16 mesophase with lower EO/PO ratios is obtained by using a blend of Pluronic F127 with Pluronic copolymer P123. Each mesopore in the cubic structure of SBA-16 has eight neighboring mesopores, in fact, the electron crystallography study shows that each mesopore is connected to its eight adjacent pores, thus forming a multi-directional network system [12]. Due to its large surface area, uniform pore structure, and interconnected three-dimensional cubic symmetry (Im3m), SBA-16 provides a highly ordered mesoporous network suitable for loading and controlled release of various therapeutic agents. These characteristics allow SBA-16 to serve as a promising nanocarrier in advanced drug delivery systems, enabling site-specific and pH-responsive release [13, 14].

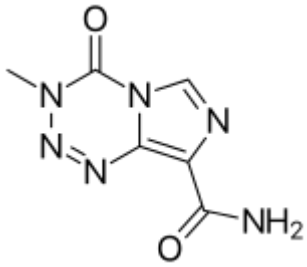

Fig 1. Chemical structure of temozolamide drug

Table 1. Physicochemical properties of temozolomide relevant to targeted drug delivery

Property	Value	Unit / Description	Relevance to Drug Delivery
Molecular weight	194.15	g/mol	Affects diffusion, loading efficiency
Log P (octanol/water)	-0.37	–	Indicates hydrophilicity; important for release profile
Water solubility	3.32	mg/mL at 25°C	Affects dissolution and loading

			into mesopores
pKa	~7.4	–	Impacts ionization at physiological pH
Stability (aqueous)	Hydrolyzes at pH > 7	–	Justifies use of controlled-release systems
Hydrogen bond donors	2	count	Influences interaction with silanol groups on SBA-16
Hydrogen bond acceptors	6	count	Affects surface binding and solubility
Polar surface area (PSA)	107.43	Å²	Related to permeability and bioavailability
Melting point	212–214	°C	Relevant during drug loading (thermal stability)
Decomposition point	~250	°C	Important for processing in mesoporous carriers

In this work, the mesostructure of SBA-16-NH_2 was first synthesized. After the structure of the target material was confirmed by the prepared analyzes (XRD, SEM, FTIR, etc.), Then the drug release studies were investigated using dialysis bag in three neutral, acidic and alkaline environments [15-17]. Also, with the help of experiment design software, 5 effective parameters in drug loading, including pH, temperature, contact time, drug concentration, and the amount of nanocomposite as a carrier, were investigated in order to obtain optimal conditions for drug loading on nanocomposite.

The novelty of this study lies in the synthesis and surface functionalization of SBA-16 mesoporous silica with amine groups (SBA-16-NH_2) to develop a highly efficient and targeted nanocarrier for the anticancer drug temozolomide. For the first time, five key parameters affecting the drug loading process—pH, temperature, contact time, initial drug concentration, and carrier dose—were simultaneously optimized using response surface methodology (RSM) based on a central composite design (CCD), which led to an exceptionally high drug loading efficiency (up to 99.99%) under mild conditions.

In addition, drug release studies were performed in three simulated physiological environments (acidic, neutral, and alkaline), demonstrating that SBA-16-NH_2 provides a pH-responsive and controlled release profile. A faster the release rate was observed under acidic conditions, while slower and sustained release occurred in neutral and alkaline media. The release kinetics data were best fitted to the pseudo-second-order model, indicating a controlled and predictable release behavior in biological systems.

To the best of our knowledge, this is one of the few studies that integrates mesoporous structure modification, statistical process optimization, and comprehensive drug release analysis to design an advanced and efficient temozolomide delivery system.

Materials and Methods

Chemicals

Pluronic surfactant F127 and Tetraethyl orthosilicate (TEOS) were supplied from Sigma Aldrich Co. (purity > 99.0%). Temozolomide drug with formula $C_6H_6N_6O_2$ purchased from Sigma-Aldrich Co. (purity: United States Pharmacopeia (USP) Reference Standard). Dialysis tubing cellulose membranes were used to perform drug release tests made by Sigma Aldrich (avg. flat width 23 mm (14000MWCO, 99.99% retention)). From sodium NaH_2PO_4 and NaO_2HPO_4 are used for the preparation of buffer solutions. All other chemicals were analytical.

Characterization

The Netherlands AXS-D8Advance model device with Cu Kα radiation source with 2θ=0.5-70° was used for X-ray diffraction (XRD) measurement. Morphology studies were performed using scanning microscope (SEM) and transmission microscope (TEM) with HITACHI and S-3400N models from Japan, respectively. The functional groups of the absorbent structure were identified using Fourier transform infrared spectroscopy (FTIR). Spectrophotometric measurements were performed by a UV/Vis spectrophotometer (Dynamica-HALO-DB-20, Germany). BET analysis was performed by nitrogen (N_2) adsorption and desorption isotherm at 77 K temperature to investigate surface area, size and pore volume (NanoSORD92 model, Japan). Thermogravimetric analysis (TGA) was performed in a nitrogen environment at a temperature of 1000 degrees Celsius and a speed of 5 revolutions per minute by TA company model Q600 made

in America. Also, in this research, pH meter (ST2100, Switzerland), magnetic stirrer (Labinco-L81ST, Netherlands), oven (Memmert, Germany), ultrasonic (Elmasonic-S, Germany) and centrifuge (Teb-X-400 rpm, Iran) were used.

Preparation of Mesoporous Silica Nanoparticles SBA-16

In a typical synthesis, 3.0 g of Pluronic P127 was dissolved in 144 mL ultrapure water and 13.9 mL 38% HCl solution, under stirring at 25°C. After half an hour, 11 mL butanol was added as co-surfactant, in order to achieve a 1: 3 mass ratio (F127: butanol). Subsequently, 15.3 mL of tetraethyl orthosilicate was added to the solution, under continuous stirring at 45°C for 24 hours. After hydrothermal treatment at 100°C for 24 hours in a Teflon autoclave, the solid was collected by filtration and air dried at 80°C under vacuum. The surfactant was removed by calcination at 550°C for 6 hours [18].

Synthesis of SBA-16-NH_2

Functionalization of silica materials with amine groups was performed under conventional anhydrous grafting conditions. For SBA-16 functionalization with 3-aminoethylaminopropyltrimethoxysilane, 1.0 g of calcined silica were heat-treated at 150 ℃ under vacuum for 12 h. After cooled down to 120 ℃, the powder was flushed under dry N_2. The solid was thereafter immersed in a solution containing 1 mL of 3-aminoethylaminopropyltrimethoxysilane precursor in 50 mL of dry toluene. The solution was heated under N_2 atmosphere at 120 ℃ for 4 h. Then, the powder was recovered by filtration, absolute ethanol washing, and drying at 100 ℃ for 12 h [19].

Temozolamide drug calibration curve

The standard solution of the drug was prepared using distilled water as the solvent due to the drug's high solubility in it, which ensures complete dissolution and accurate concentration for analytical purposes.

Solutions with specific concentrations (10-100 ppm) were prepared from the mother solution with a concentration of 1000 ppm of temozolamide and the absorbance of the desired solutions was read by UV-Vis device at the maximum wavelength of temozolamide (329 nm). By plotting the absorbance-concentration diagram, the best line equation was obtained to obtain theunknown concentrations (Fig 2).

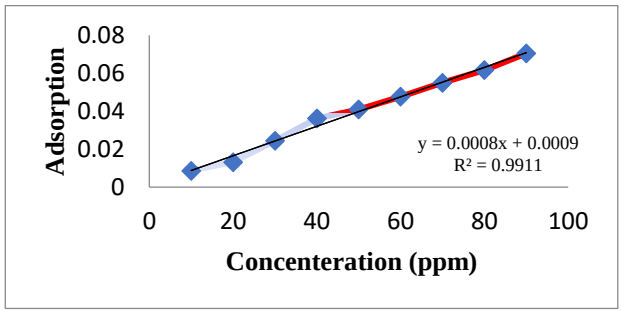

Fig 2. Adsorption calibration curve of temozolamide drug

Drug Loading

To load the drug onto SBA-16-NH_2 nanoparticles, 10 ml of temozolamide was pipetted, then the pH value suggested by the experimental design software was adjusted in each experiment using 0.1 M hydrochloric acid and sodium hydroxide. The amount of nanocarrier was weighed and added to the drug solution, then the defined temperature was applied and the drug solution along with the nanocarrier was placed on a magnetic stirrer for a specified time. After the stirring time was over, the nanocarrier was separated from the drug using a centrifuge. The concentration of the absorbed drug was measured using a UV device at the maximum wavelength of the drug (maxλ = 329). The percentage absorbed was calculated using equation 1:

$$\%\text{Load} = \frac{(C_0 - C_e)}{C_0} \times 100 \qquad (1)$$

Where C_0 and C_e are the initial and equilibrium concentrations of the drug, in mg/L, respectively.

The pH_{PZC} of SBA-16-NH_2

In the process of surface adsorption, at pH_{PZC} the electric charge density on the surface is zero. When the pH of the environment is lower than the pH_{PZC} value, there are more protons on the surface, and the surface of adsorbent becomes positively, which is able to adsorb anions. Conversely, if the pH is higher than pH_{PZC}, the surface becomes negatively charged, which is important in absorbing harmful cations. To determine pH_{PZC}, 0.01 g of SBA-16-NH_2 was dissolved in 15 ml of distilled water. Solutions of SBA-16-NH_2 were prepared and each solution was adjusted to a pH (pH_i= 2-12) by HCl and NaOH. After stirring the solution for 1 hour, the pH was read again (pH_f) [20]. By drawing the graph of pH_f *vs.* pH_i (Fig 3), the pH_{PZC} was obtained.

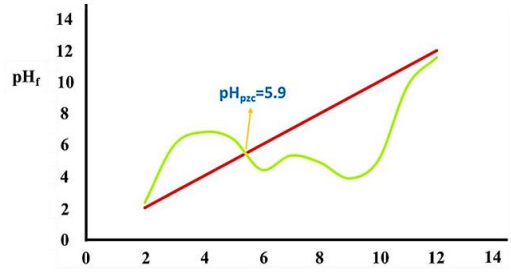

Fig 3. The pH_{PZC} of SBA-16-NH_2 adsorbent

Experiment design using the response surface method

Response surface method (RSM) is a statistical method used in the development of statistical models to solve various equations. This method is based on predicting the functional relationship between the response and the experimental variables [21]. It also optimizes variables. The response surface method uses a series of designed experiments and obtains an optimal response for the entire method that is dependent on the process variables. Central composite design or CCD is the most common method used when optimizing process related parameters [22].

In this research, experiment design, statistical data analysis using Stat-Ease Design-Expert software (version 11), response surface method as a mathematical and statistical tool to optimize variables affecting adsorption such as solution pH, adsorbent amount, the initial concentration of the drug, contact time and temperature for the adsorption of the cefixime drug were performed as the response (output). Table 1 shows different experimental levels of independent factors and their codes. Table 2 basically consists of 2^n factorials and $2 \times n$ axial paths along with the number of central points (p). Eq 2 is used to calculate the number of test runs based on the number of input variables:

$$N_p = [2^m + (2 \times m) + p] \quad (2)$$

where Np indicates the number of necessary test executions, m indicates the number of variables affecting the output of the process. In this research, the value of m is equal to 5.

Table 2. Different levels for independent parameters affecting drug absorption

code	independent parameters	unit	-2	1-	0	1+	+2
A	pH	-	2	4	6	8	10
B	Absorbent dose	g	0.01	0.02	0.03	0.04	0.05
C	Drug concentration	ppm	10	20	30	40	50
D	Temperature	℃	30	40	50	60	70
E	Contact time	min	10	20	30	40	50

The central composite design consists of 3 steps, which include starting the experiment design, calculating the model coefficients, predicting the model's behavior, and calculating the results [23]. The experiments lead to the creation of an empirical model that calculates the functional behavior based on the input parameters along with their related combinations, and a second-order polynomial model is obtained for the analysis and prediction of drug loading as shown in Eq 3:

$$Y = \beta_0 + \sum_{i=1}^{5} \beta_i X_i + \sum \beta_{ij} X_i X_j \quad (3)$$

where Y and (X_i and X_j) respectively represent the response of drug absorption in terms of percentage and coded independent factors. β_0 is a constant value, while β_i, β_{ii}, and β_{ij} represent the linear, quadratic, and interactive coefficients of the input independent variables, respectively [24]. A total of 50 runs by the response surface model were proposed by the software to investigate the effects of 5 independent factors on drug absorption as presented in Table 3.

Table 3. Experiments suggested for cefixime drug adsorption

Run	A:pH	B:comp. dose	C:cons. drug	D:temp.	E:cont. time	load
	-	g	ppm	C	Min	%
1	10.00	0.03	30.00	50.00	30.00	48.00
2	4.00	0.02	40.00	60.00	20.00	80.50
3	6.00	0.03	10.00	50.00	30.00	68.50
4	8.00	0.04	20.00	40.00	40.00	61.50
5	8.00	0.02	20.00	40.00	20.00	88.75
6	6.00	0.05	30.00	50.00	30.00	61.00
7	8.00	0.04	40.00	40.00	20.00	80.25
8	6.00	0.03	30.00	50.00	30.00	68.50
9	8.00	0.04	20.00	40.00	20.00	58.00
10	8.00	0.02	40.00	60.00	20.00	90.25
11	4.00	0.02	40.00	40.00	20.00	73.50
12	6.00	0.03	50.00	50.00	30.00	57.10
13	8.00	0.02	20.00	60.00	40.00	99.50
14	2.00	0.03	30.00	50.00	30.00	79.75
15	6.00	0.03	30.00	50.00	30.00	99.99
16	4.00	0.04	20.00	60.00	40.00	80.25
17	6.00	0.03	30.00	50.00	30.00	99.00
18	4.00	0.04	20.00	40.00	40.00	80.50
19	6.00	0.03	30.00	50.00	30.00	83.00
20	4.00	0.02	20.00	60.00	20.00	95.00
21	4.00	0.04	20.00	60.00	20.00	90.50
22	4.00	0.02	20.00	40.00	20.00	90.00
23	4.00	0.02	40.00	40.00	40.00	78.50
24	6.00	0.03	30.00	30.00	30.00	66.00
25	8.00	0.02	40.00	40.00	40.00	70.25
26	6.00	0.03	30.00	50.00	10.00	62.00
27	8.00	0.02	40.00	60.00	40.00	96.00
28	4.00	0.04	20.00	40.00	20.00	64.75
29	8.00	0.04	20.00	60.00	20.00	81.50
30	6.00	0.03	30.00	50.00	30.00	66.30
31	8.00	0.02	40.00	40.00	20.00	86.00
32	4.00	0.02	40.00	60.00	40.00	79.00

33	6.00	0.03	30.00	50.00	30.00	67.50
34	8.00	0.04	20.00	60.00	40.00	58.25
35	8.00	0.02	20.00	60.00	20.00	88.00
36	4.00	0.02	20.00	40.00	40.00	89.00
37	4.00	0.04	40.00	60.00	40.00	76.00
38	4.00	0.04	40.00	60.00	20.00	58.50
39	8.00	0.02	20.00	40.00	40.00	86.20
40	4.00	0.02	20.00	60.00	40.00	80.50
41	6.00	0.03	30.00	50.00	30.00	78.00
42	6.00	0.03	30.00	50.00	50.00	68.50
43	6.00	0.03	30.00	70.00	30.00	79.50
44	6.00	0.03	30.00	50.00	30.00	91.50
45	4.00	0.04	40.00	40.00	40.00	62.50
46	8.00	0.04	40.00	60.00	40.00	80.75
47	6.00	0.01	30.00	50.00	30.00	68.50
48	8.00	0.04	40.00	40.00	40.00	68.00
49	4.00	0.04	40.00	40.00	20.00	88.00
50	8.00	0.04	40.00	60.00	20.00	55.00

Drug release

In this study, drug release was performed by dialysis process. In the dialysis process, first the dialysis bag was cut according to the width of the dialysis bag and the volume of the solution. After that, it was boiled in 2% sodium bicarbonate solution for 10 minutes to prepare. Then, the end of the dialysis bag was closed with special clamps and the temozolamide drug solution along with the SBA-16-NH_2 nanocarrier was transferred into the bag, and its beginning was closed again with special clamps so that there was no leakage. Three acidic, alkaline and neutral environments were prepared as simulated body environments with a volume of 500 ml each and the dialysis bag was placed in them. This set was placed on a magnetic stirrer at 37 degrees Celsius. Drug release experiments were tested at times of 1, 2, 3, 4, 12, 24, 48 and 72 hours. In dialysis, the drug permeates from the nanocarrier into the dialysis bag membrane and diffuses into the buffer solution. The release rate of temozolamide from the SBA-16-NH_2 nanocarrier was calculated using eq 4.

$$\%\text{release} = \frac{\text{Weight of drug in solution}}{\text{Weight of medicine in SBA}-16-\text{NH2}} \times 100 \qquad (4)$$

Results and Discussions

Characterization of mesostructure of SBA-16-NH_2

The FTIR spectrum of SBA-16 and SBA-16-NH_2 can be seen in Fig 4a. As shown in Figure 4a, a broad peak at 3441.12 cm^{-1} is associated with the symmetric stretching vibration of the O-H bond of the Si-OH silanol groups. Also, the peak observed at 1630.95 cm^{-1} is associated with the stretching and bending vibrations of the water molecules adsorbed on the SBA-16 surface. The peaks at 463.52 cm^{-1}, 805.2 cm^{-1} and 1086.21 cm^{-1} are associated with the symmetric and asymmetric Si-O-Si bending, stretching and bending vibrations, respectively. The above data confirm that the synthesized material is a silicate mesoporous [25]. The observed band at 1085.30 cm^{-1} is related to the asymmetric stretching vibrations of Si-O-Si and around 797.37 cm^{-1} and 949.10 cm^{-1} is dedicated to the symmetric stretching vibrations of the Si-O-Si bond. Also, the bands observed in the region of 471.94 cm^{-1} represent tetrahedral silica due to the presence of SiO_4 units. The broad band of 16.3414 cm^{-1} refers to the O-H stretching vibration mode of silanol groups. Bands assigned to C-H stretching vibrations of propyl chains were observed around 2930 cm^{-1} in the spectrum of the sample containing amine. (C-H)ν and (C-H)δ deformation vibrations in methyl groups were observed in the regions of 1463.39 cm^{-1} and 1353 cm^{-1} in the spectrum of the sample containing amine [26]. Also, in the XRD analysis related to mesopore SBA-16 and SBA-16-NH_2 (Fig 4b), a very strong peak at $2\theta = 20\text{-}30°$. corresponding to the (110) plane, and the next three weak peaks at a higher angle, corresponding to the (211) plane, are observed. Which confirms the presence of a cubic structure of space group Im3m [27]. Fig 4d shows the scanning electron microscope (SEM) image of the surface of the synthesized SBA-16 and SBA-16-NH_2 samples. According to this micrograph, it can be concluded that the synthesized samples of SBA-16 and SBA-16-NH_2 has spherical and homogeneous morphology. Also, the size of the pores is in the range of 2-50 nm, which proves that the synthesized material is a mesoporous one [28]. The low-angle X-ray diffraction (XRD) pattern of SBA-16-NH_2 confirms the presence of a well-ordered mesoporous structure with a three-dimensional cubic symmetry of Im3m, characteristic of SBA-16 materials. Distinct diffraction peaks are observed in the low 2θ range (typically between 0.8° and 1.5°), corresponding to the reflections from various (hkl) planes of the cubic mesoporous network. The presence of these peaks indicates a highly ordered and coherent mesoporous framework with cubic geometry. After functionalization with amino groups (NH_2), slight changes in the intensity and position of these peaks are noticed, indicating that the original mesoporous structure is retained and the amino groups are successfully grafted onto the pore walls. The minor reduction in peak intensity is generally attributed to the partial filling of the mesopores by the grafted amino groups, which affects the diffraction pattern slightly. Therefore, the low-angle XRD results confirm that SBA-16-NH_2 maintains its three-dimensional cubic Im3m mesoporous structure, and the surface functionalization does not lead to structural collapse (Fig. 4c). TEM image taken of the SBA-16-NH_2 mesostructure at a magnification of 100 nm is shown in Fig. 4e. This image shows a highly ordered cage-like arrangement of

mesopores. Fig 4f shows the adsorption-desorption isotherm diagram of SBA-16-NH_2. As can be seen, this nanocomposite has a type IV isotherm and the adsorption curve does not coincide with the desorption curve and forms a ring called hysteresis. When a compound forms a hysteresis ring in its isotherm diagram, it can be said that that compound has 100% mesopores. Also, using the adsorption-desorption isotherm diagram and the hysteresis ring formed, the geometry of the pores can be identified. According to the diagram, the hysteresis ring is of type H1. Therefore, the pores have a cylindrical geometry [29]. Table 4 shows the results of BET analysis of mesoporous SBA-16-NH_2. The results indicate that the specific surface area of SBA-16-NH_2 is 258.64 m^2/g. Also, the average particle diameter and pore volume were 4.098 nm and 0.5876 cm^3/g, respectively. Therefore, it can be concluded that the synthesized SBA-16-NH_2 is mesoporous [30]. The thermal stability of the samples was determined by thermogravimetric analysis (Fig 4g). The mass loss between room temperature and 200°C corresponds to the release of absorbed moisture. It should be noted that mass loss in this temperature range is reduced as a result of modification with amine groups. At higher temperatures, thermal decomposition of the amine ligands took place and the decomposition was completed at 800°C. For samples modified with amine groups, only one main peak was observed at 400 ℃ [31].

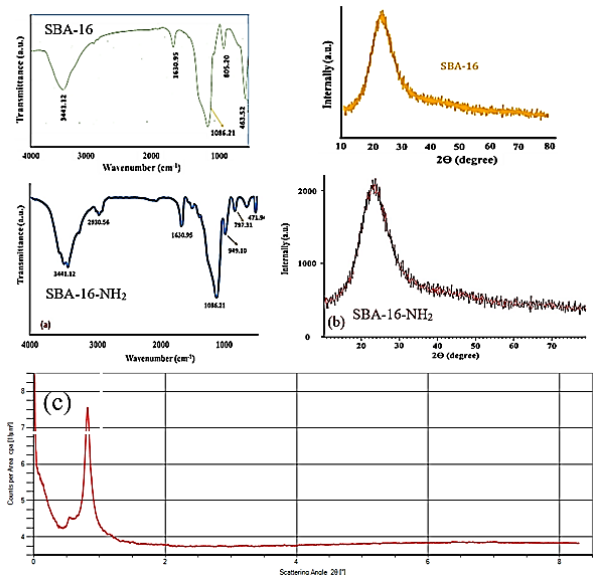

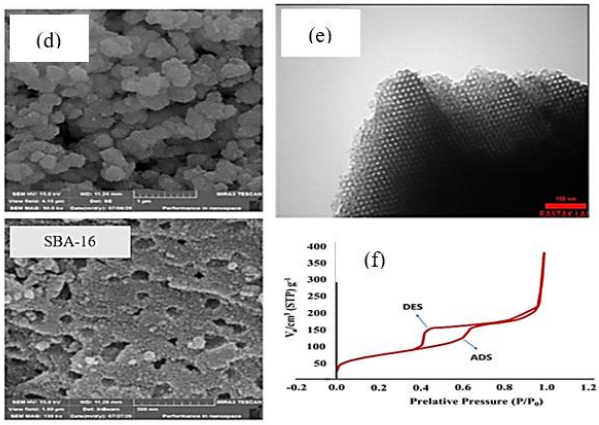

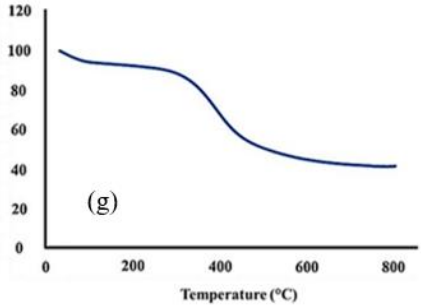

Fig 4. (a) FTIR spectrum, (b) XRD analysis, (c) low angle XRD pattern, (d) SEM image, (e) TEM image, (f) BET analysis and (g) TGA analysis of SBA-16-NH_2

Table 4. BET analysis results

BET table

V_m	59.423	[cm^3(STP) g^{-1}]
$a_{s,BET}$	258.64	[m^2 g^{-1}]
C	174.6	
Total pore volume(p/p_0=0.988)	0.5876	[cm^3 g^{-1}]
Average pore diameter	4.087	[nm]

Statistical analysis

After the tests, the results are given to the software to provide the best model for evaluating and describing the data. The proposed model of the software was among the four linear, interactive, quadratic and cubic models, the quadratic model was the most consistent with the responses. Because the best and most suitable model is determined based on the p-value values and regression coefficients [32]. As can be seen in Table 5, the quadratic model has a p-value less than 0.05 and the highest regression coefficient compared to the other 3 models.

Table 5. Results of statistical analysis of temozolamide drug loading on SBA-16-NH_2 nanocarrier

Source	Seq. p-value	Lack of Fit p-value	Adj. R^2	Pred. R^2	
Linear	< 0.0001	< 0.0001	0.9020	0.8852	
2FI	0.0011	< 0.0001	0.9419	0.9404	
Quadratic	< 0.0001	0.0685	0.9953	0.9905	Suggested
Cubic	0.0690	0.1770	0.9972	0.9839	Aliased

The results of analysis of variance (ANOVA) for drug loading are shown in Table 5, where a smaller P-value (P-value less than 0.05 indicates that the model terms are significant) and a higher F-value indicate a more significant effect of the model conditions. Statistically, a small p-value and a large F-value indicate the importance of a model or a parameter [33]. As shown in Table 6, the quadratic model is highly significant for temozolamide drug loading due to the high F-value (522.04) and very low p-value (p<0.0001) [34]. Based on the F-values, the independent parameters that affect the drug loading efficiency of temozolamide are pH, temperature, nanocarrier dose, drug concentration, and contact time, respectively, indicating that pH is the most influential parameter on drug loading and contact time is the least influential. In addition, the interaction between A and C and B and C was significant.

Table 6. Results of ANOVA analysis of variance of temozolamide drug loading on SBA-16-NH_2 nanocarrier

Source	Sum of Squares	df	Mean Square	F-value	p-value	
Model	8246.91	20	412.35	522.04	< 0.0001	Sig.
A	6957.73	1	6957.73	8808.63	< 0.0001	
B	177.45	1	177.45	224.66	< 0.0001	
C	118.51	1	118.51	150.03	< 0.0001	
D	212.29	1	212.29	268.76	< 0.0001	
E	76.31	1	76.31	96.62	< 0.0001	
AB	9.52	1	9.52	12.05	0.0016	
AC	65.12	1	65.12	82.45	< 0.0001	
AD	1.69	1	1.69	2.14	0.1545	
AE	2.56	1	2.56	3.24	0.0823	
BC	205.79	1	205.79	260.54	< 0.0001	
BD	10.29	1	10.29	13.03	0.0011	
BE	31.50	1	31.50	39.88	< 0.0001	
CD	29.55	1	29.55	37.41	< 0.0001	
CE	14.65	1	14.65	18.54	0.0002	
DE	23.38	1	23.38	29.59	< 0.0001	
A^2	81.44	1	81.44	103.11	< 0.0001	
B^2	52.40	1	52.40	66.34	< 0.0001	
C^2	19.61	1	19.61	24.83	< 0.0001	
D^2	87.95	1	87.95	111.34	< 0.0001	
E^2	69.18	1	69.18	87.58	< 0.0001	
Res.	22.91	29	0.7899			
Lack of Fit	20.73	22	0.9421	3.03	0.0685	not sig.
Pure Error	2.18	7	0.3114			
Cor Total	8269.82	49				

The appropriateness of the equation of the proposed model (polynomial) was checked with the help of R^2, R^2 Adj. and R^2 Pred. A high value of R^2 indicates a better fit of the equation with the experimental data. According to Table 7, the values of predicted R^2 and adjusted R^2 are 0.9940 and 0.9967, respectively. The closer these values are to one, they confirm the adequacy of the quadratic model for more drug loading. Also, the sum of squares of R or R^2 is equal to 0.9953. This number means that 99.53% of the response variable changes can be explained using the proposed software model [35].

Table 7. Regression coefficients of the quadratic model

Std. Dev.	0.8887		R^2	0.9972
Mean	76.67		Adjusted R^2	0.9953
C.V. %	1.16		Predicted R^2	0.9905
			Adeq Precision	91.5924

The experimental results can be verified by analyzing the graphs obtained from the response surface model by model accuracy plots including experimental vs. predicted values, standard residuals vs. predicted values, and standard residuals vs. experimental values. The high agreement between the experimental and predicted values of the high percentage of drug loading by the SBA-16-NH_2 nanocarrier is shown in Fig 5a, as shown in Figure 8a. The experimental values of drug loading efficiency and the predicted values have a high degree of agreement. It can be inferred from Figure 5a that the predicted points and the experimental results are mostly close to each other [36]. This observation indicates that the experimental results are very acceptable for this research. Fig 5b and c show the standard residuals vs. the experimental and predicted values, confirming that the observed errors are normally distributed within the confidence interval ± 3.67. From Fig 5b, it can be seen that the points are scattered around the horizontal line, indicating that there is no significant change between the actual and predicted [37].

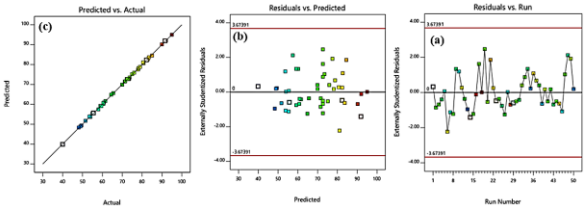

Fig 5. (a). Predicted values vs. experimental values, (b). Standard balance vs. predicted values, (c). Standard vs. experimental values

Effect of parameters on drug loading

Determining pH is one of the most important aspects in drug loading at different pH levels. At pH less than pHzpc, due to the high concentration of H^+ ions in the medium, the surface charge of the adsorbent is positive [38]. Therefore, positively charged adsorbents can effectively adsorb drug molecules with negative charges. However, at pH higher than pH_{pzc}, due to the high concentration of OH^- ions, the surface charge of the adsorbent becomes negative. As a result, a repulsion is created between the negatively charged adsorbent and the negatively charged drug molecules, and the drug loading rate decreases. Experiments were conducted for the drug loading efficiency of temozolamide in the pH range between 2 and 10. The results are shown in Figure 9a. In acidic conditions, the drug loading efficiency increased and decreased in basic conditions. High temozolamide loading on SBA-16-NH_2 was obtained at pH = 2.73. The increased drug loading in acidic conditions is related to the electrostatic attraction of temozolamide with SBA-16-NH_2. At lower pH (pH = 2.73), increased electrostatic attraction between the temozolamide drug and the SBA-16-NH_2 surface leads to increased temozolamide loading.

Fig 6b shows the effect of adsorbent dose on the adsorption of temozolamide by SBA-16-NH_2 nanosorbent. The loading percentage increases with increasing dose up to 0.045 g. The increase in loading percentage is due to the increase in the active sites of the adsorbent. However, with further increase in the adsorbent dose, the loading percentage remains quite constant because at higher adsorbent dose, the concentration of temozolamide molecules in the solution is not sufficient to cover all the adsorption sites on the adsorbent surface. Therefore, the equilibrium adsorbent dose for temozolamide was 0.045 and this value was used for subsequent experiments [39].

The effect of initial drug concentration of temozolamide on the adsorption efficiency was investigated in the drug concentration range of 10-50 mg/L. The present study shows that the nanocarrier can adsorb up to 10 mg/L of drug. The effect of initial drug concentration factor is determined by the interaction between the binding sites available on the adsorbent surface and the drug concentration. In most cases, with increasing initial drug concentration, the ratio of loaded drug decreases. This can be due to the saturation of the adsorbent surface with adsorption sites. When the drug concentration is low, there are empty active sites on the adsorbent surface. However, with increasing concentration, the active sites required for drug adsorption are not available. In other words, with increasing initial drug concentration, the residual concentration of drug molecules will be higher. While at lower concentrations, the ratio of initial number of drug molecules to unoccupied adsorption sites is minimal. Fig 6c shows the effect of initial drug concentration (10 mg/L) [40].

The adsorption of temozolamide onto SBA-16-NH_2 nanocarrier was investigated at temperatures of 30, 40, 50, 60 and 70 K (Fig 6d). The results showed that the drug release rate decreased with increasing temperature. This decrease in loading can be attributed to changes in Gibbs free energy. With increasing temperature, the enthalpy and entropy changes become negative, and according to the thermodynamic relationship $\Delta G=\Delta H-T\Delta S$, the entropy becomes positive, resulting in a positive Gibbs free energy. Therefore, at low temperatures the adsorption process is spontaneous [41].

The relationship between temozolamide loading and contact time is shown in Fig 6e. This figure shows that the time required to reach equilibrium adsorption is directly proportional to the loading. Experiments showed that in the first 10 min, from 0 to 10 min, temozolamide loading increased rapidly due to the large amount of mesoporous particle surface area available for loading. Then, from 10 to 50 min, temozolamide drug loading decreased with time, which was due to the decrease in the availability of mesoporous particle surface area for loading. However, the drug loading curve became almost horizontal after 50 min, indicating that the mesoporous particle surfaces were full (saturated), or in other words, they had reached the equilibrium adsorption level. The best loading time was the first 10 min [42].

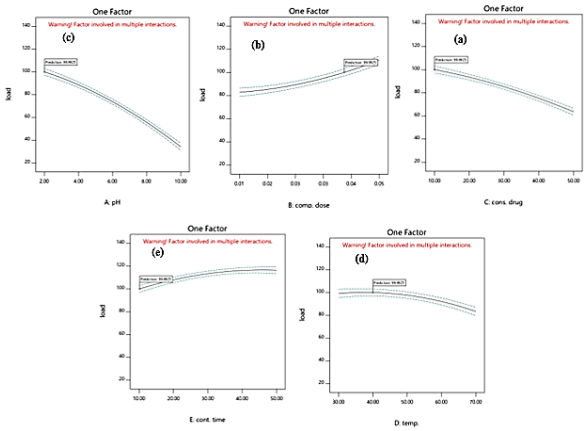

Fig 6. Effect of independent parameters on the amount of drug loading, (a). effect of pH, (b). effect of nanosorbent dosage, (c). effect of drug concentration, (d). effect of temperature, (f). effect of contact time

Interaction effects of independent variables

The interaction effects of the dependent variables on drug loading are presented in Fig 7. According to Figure 10a, with increasing the adsorbent dose from 0.01 to 0.05 g/L and decreasing the pH from 10 to 2, the drug loading increases, while the highest drug loading was obtained at pH = 2.73 and adsorbent dose of 0.045 g/L and the optimum pH for drug loading was 2.73 when other parameters were kept constant. In Fig 7b, when the initial drug concentration increased from 10 to 50 mg/L, the percentage of drug loading decreased at all adsorbent doses. However, the interaction effect between drug loading concentration and adsorbent dose was statistically insignificant, especially at low adsorbent doses. Fig 7c shows the interaction effect between pH and drug concentration. As is evident from this figure, while the pH and initial drug concentration decreased, the drug loading increased. Therefore, the interaction effect of pH and drug concentration is significant. The decrease in drug loading with increasing initial drug concentration can be attributed to the fact that with increasing drug concentration, the number of active sites on the adsorbent surface is not sufficient to adsorb all drug molecules, thus the drug loading decreases [43, 44].

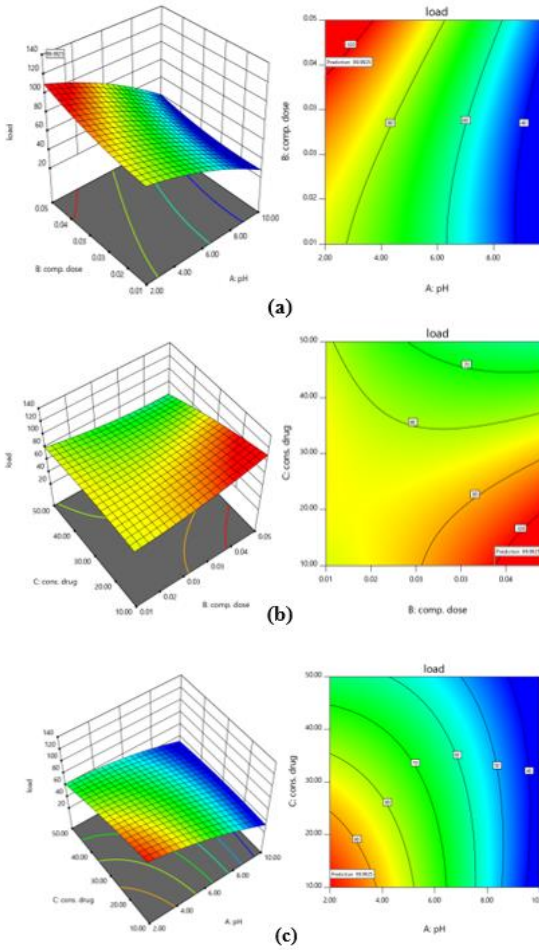

Fig 7. The mutual effect of independent parameters on the rate of temozolamide loading

Optimization studies

To evaluate the optimal conditions for maximum drug loading, 5 variables pH, nanocarrier amount, initial drug concentration, temperature and contact time were studied within the range suggested by the software. The experimental design software suggested pH = 2.73, nanocarrier dose 0.045 g, drug concentration 10 mg/L, temperature 30°C and contact time 10 min as the optimal conditions to achieve maximum drug loading of 99.99% with a desirability of 1. The experiments were repeated under the predicted optimal conditions. The results are reported in Table 8 where the experimental data were very close to the predicted value confirming the validity and adequacy of the model.

Table 8. Optimal values of independent variables for maximum absorption of temozolamide

parametr	pH	Ads. dose	drug cons.	Temp.	Cont. time	Load %

						Real	Pred.
Opt. value	2.73	0.045	10.00	30.00	10.00	98.82	99.99

Adsorption isotherm

The adsorption isotherm determines the transfer of the adsorbed material to the adsorbent in equilibrium conditions. Interactions between drug and adsorbent molecules and maximum adsorption capacity can be described by equilibrium isotherms. Therefore, Langmuir, Freundlich and Temkin models were studied to describe the adsorption of temozolamide on SBA-16-NH_2 adsorbent (Fig 8). Adsorption isotherm experiments were performed under optimal conditions and different drug concentrations of 10, 20, 30, 40 and 50 mg/L.

Langmuir isotherm describes the monolayer and homogeneous adsorption of drug molecules on the adsorbent surface [45]. The linear form of the Langmuir isotherm is expressed as eq 5:

$$\frac{1}{q_e} = \frac{1}{q_m} + \left(\frac{1}{q_m K_L}\right)\frac{1}{C_e} \quad (5)$$

where q_e (mg/g), C_e (mg/L), q_{max} (mg/g) and K_L(l/mg) and respectively the amounts of absorbed drug in the equilibrium state, the equilibrium concentration of the absorbed substance, the maximum absorption capacity and are Langmuir equilibrium constants. K_L and q_{max} values are calculated from the graph of $1/C_e$ versus $1/q_e$ [46].

The Freundlich isotherm assumes that drug adsorption on a heterogeneous adsorbent surface is multilayered. The linear form of the Freundlich isotherm is as described in eq 6:

$$\log q_e = \log k_F + \frac{1}{n}\log C_e \quad (6)$$

where n (l/mg) and K_F (mg/g) are the Freundlich constant and absorption intensity, respectively. K_F and n can be determined from the linear plot of log q_e versus log C_e [47].

Temkin isotherm is used for adsorbents in which the active sites of adsorption are not the same in terms of energy and chemical adsorption that is carried out in the form of a single layer. The linear form of Temkin isotherm is defined based on eq 7:

$$q_e = B_1 \ln C_e + \ln K_T \quad (7)$$

K_T is the Temkin isotherm constant and B_1 depends on the heat of the surface adsorption process. The values of B_1 and B_1 $\ln K_T$ are calculated by drawing the graph of $\ln C_e$ against q_e and determining the equation of the line using the slope and width of the origin [48].

The isotherm parameters for the adsorption of temozolamide drug on SBA-16-NH_2 adsorbent are given in Table 9, where the highest correlation coefficient of corresponds to the Langmuir isotherm, which shows that the adsorption data are well fitted with the Langmuir isotherm.

Table 9. Isotherm parameters for absorption of temozolamide drug on SBA-16-NH_2 nanosorbent

Parameter	Adsorption isotherm
Langmuir	
q_{max} (mg.g^{-1})	28.57
K_L (l/mg)	0.55
R^2	0.9936
Freundlish	
n	2.93
K_F ($mg^{-1(1/n)}L^{1/n}g^{-1}$)	10.43
R^2	0.8313
Temkin	
B	4.9461
K_T (l/mg)	1.61
R^2	0.9387

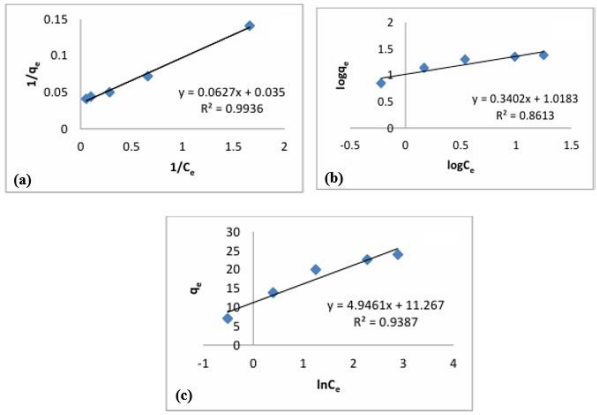

Fig 8. Langmuir isotherm, Freundlich isotherm and Temkin isotherm of absorption of temozolamide drug on SBA-16-NH_2 nanosorbent

Adsorption thermodynamics

Thermodynamic studies are necessary to evaluate whether the adsorption process is spontaneous or not. It also helps to identify whether the absorption process is endothermic or exothermic. Adsorption thermodynamics at different temperatures were studied to estimate the effect of temperature on the drug absorption process [49]. Various thermodynamic parameters, such as enthalpy changes ΔH^o, entropy changes ΔS^o, and Gibbs free energy changes ΔG^o, can be evaluated from Eq 8 to 11.

$$K = \frac{q_e}{C_e} \quad (8)$$

$$\Delta G° = -RT\ln K \quad (9)$$

$$\Delta G° = \Delta H° - T\Delta S° \quad (10)$$

$$\ln K = \frac{\Delta H^\circ}{RT} + \frac{\Delta S^\circ}{R} \quad (11)$$

where, K represents the equilibrium constant, T is the adsorption temperature (K) and R represents the universal gas constant (8.314 J/mol.K). Using the slope and width from the origin of the 1/T diagram, the value of ΔH^o and ΔS^o is obtained in terms of lnK.

According to Fig 9, the negative value of enthalpy showed that the absorption process of temozolamide drug on SBA-16-NH_2 adsorbent is exothermic. The amount of entropy also decreases in the absorption process due to the location of the absorbed molecules on the absorbent surface as a result of their regularization, the negative sign of entropy is also for this reason. The negative values obtained for Gibbs free energy indicate the spontaneity of the absorption process of temozolamide drug by SBA-16-NH_2 adsorbent, according to the obtained results, the value of ΔG^o increases with decreasing temperature, which is based on eq 8 and with Considering the negative values of entropy and enthalpy, the reduction of Gibbs free energy is not far from expected [50].

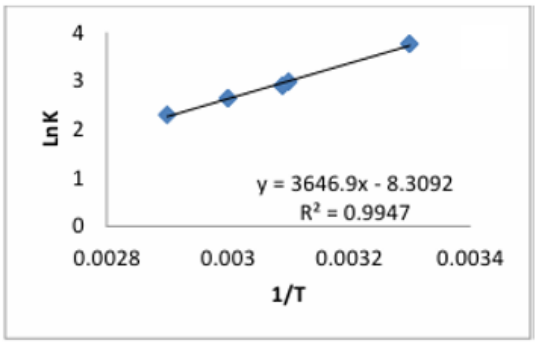

Fig 9. Thermodynamic diagram of temozolamide drug adsorption on SBA-16-NH_2 nanosorbent

Table 10. Values of thermodynamic parameters of drug adsorption

Temp. (K)	ΔH° ($Kj.mol^{-1}$)	ΔS° ($Kj.mol^{-1}$)	ΔG° ($Kj.mol^{-1}$)	R^2
303			-940	
313	-30.32	-0.069	-8.70	0.9947
323			-8.03	
333			-7.30	
343			-6.60	

Adsorption kinetics

Fast reaction speed, short contact time and significant adsorption capacity are the necessary conditions for an effective adsorption process. To better clarify the characteristics of the adsorption process, 3 kinetic models, pseudo first order, pseudo second order and Higuchi kinetics were used in optimal conditions to describe the change of the effective number of active sites on the surface of the adsorbent during adsorption (Fig 10).

The pseudo-first order model is expressed as Eq. 12:

$$\ln(q_e - q_t) = -k_1 t - \ln q_e \quad (12)$$

where q_e (mg/g) and q_t (mg/g) are adsorption capacity at the moment of equilibrium and time t. k_1 (min^{-1}) and t (min) are the reaction rate and time constants, respectively. K_1 and qe are calculated from the linear graph of ln ($q_e - q_t$) versus time, respectively [51].

The pseudo-second order model is expressed by Eq. 13:

$$\frac{t}{q_t} = \frac{1}{k_2 q_e^2} + \frac{1}{q_e} t \quad (13)$$

Where k_2 (g/mg min) is the pseudo-second order rate constant. q_e and k_2 are determined from the slope and width from the origin of the linear graph of t/q_t against t [52].

Kinetics of Higuchi model assumes that the intraparticle diffusion of drug molecules on the adsorbent is the rate-limiting step in the absorption process [53]. The Higuchi kinetics model is expressed as Eq. 14:

$$q_t = k_{id}\sqrt{t} + C \quad (14)$$

The kinetic parameters for the load of temozolamide drug by SBA-16-NH_2 nanoadsorbent are given in Table 11. The

correlation coefficients in this table show that the absorption data follow the pseudo second order model (R^2 = 0.9953). The kinetic parameters extracted (Table 11) indicate that although all three models fit the data well, the highest correlation coefficient R^2 corresponds to the pseudo-second-order model (0.9953), suggesting the predominance of chemisorption in the process. The pseudo-first-order model also exhibits a high correlation coefficient (0.9838), while the Higuchi model performs slightly less well (0.9813). Therefore, it can be concluded that the adsorption mechanism involves a combination of surface adsorption and intraparticle diffusion, with chemisorption playing the dominant role.

Table 11. Kinetic parameters for the adsorption of the drug temozolamide on SBA-16-NH_2 nanosorbent

Parameter	Kinetic model
pseudo first order	
q_e (mg.g^{-1})	1.53
k_1 (min^{-1})	-4.62
R^2	0.9838
pseudo-second order	
q_e (mg.g^{-1})	15.01
k_2 (mg.g^{-1}.min^{-1})	0.0019
R^2	0.9953
Higuchi model	
C (mg.g^{-1})	7.5261
k_{id} (mg.g^{-1}.min$^{-1/2}$)	0.4201
R^2	0.9813

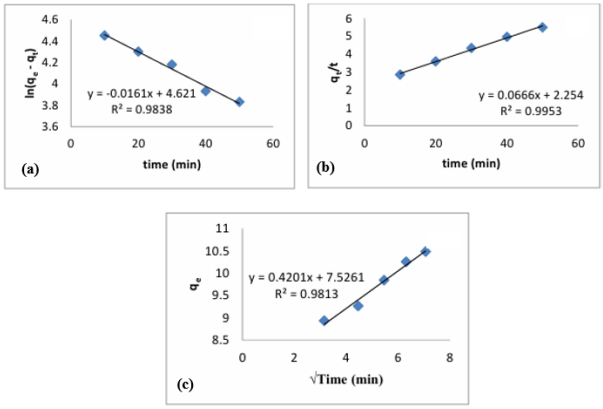

Fig 10. pseudo-first-order, pseudo-second-order, and intraparticle kinetics of temozolamide drug adsorption

Drug release

The drug release curve in three acidic environments, alkaline environment and neutral environment is seen in Fig 11. As can be seen, the release rate of temozolamide in acidic environment with pH = 4.8 is higher compared to alkaline and neutral environments with pHs of 7.4 and 6.8, respectively, so that after 72 hours, 44% of the drug in acidic environment, 40% in alkaline environment and 38.9% in neutral environment of temozolamide drug has been released from SBA-16-NH_2 nanocarrier. The increase in drug release in acidic environment is due to the higher solubility of temozolanide at low pH. on the other hand, SBA-16-NH_2 is a cation exchange compound and at low pH it immediately exchanges temozolamide with H^+ of the environment. Also, in the initial hours of release, the drug release is explosive due to the release of drug molecules adsorbed on the surface of the nanocarrier, then the drug release becomes slow and stable due to the release of drug molecules adsorbed inside the pores of the nanocarrier. These results are consistent with the studies of Zhang in 2012 for drug release from mesoporous silica nanoparticles [54-57]

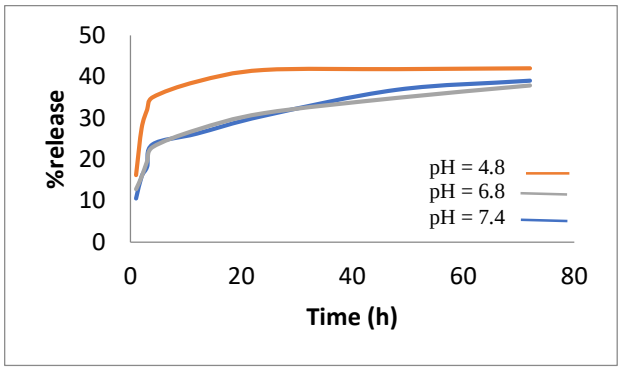

Fig 11. Release of temozolamide in three acidic, alkaline and neutral environments

Drug release kinetics

The drug release data were analyzed to determine the release kinetics using pseudo-first-order, pseudo-second-order, and Higuchi models. The results of the R^2 values of the obtained plots showed that there was a good fit between the experimental data for all three environments and the pseudo-second-order model (Fig 12).

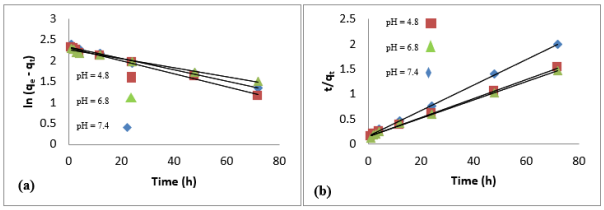

Fig 12. (a) Pseudo-first-order kinetics, (b) Pseudo-second-order kinetics of temozolamide drug release

Table 12. Kinetic parameter values for temozolamide drug release from SBA-16-NH_2 nanocarrier

Parameter	Kinetic model
Pseudo-first-order kinetics	
Neutral environment	
q_e (mg.g^{-1})	0.815
k_1 (h^{-1})	-0.0109
R^2	0.9878
Alkaline environment	
q_e (mg.g^{-1})	0.836
k_2 (mg.g^{-1}.min^{-1})	-0.0136
R^2	0.9856
Acidic environment	
q_e (mg.g^{-1})	0.845
k_{id} (mg.g^{-1}.min$^{-1/2}$)	-0.0154
R^2	0.9**895**
Pseudo-second-order kinetics	
Neutral environment	
q_e (mg.g^{-1})	54.34
K_2 (g/mg.h^{-1})	0.0022
R^2	0.9970
Alkaline environment	
q_e (mg.g^{-1})	39.91
K_2 (g/mg.h^{-1})	0.0040
R^2	0.9980
Acidic environment	
q_e (mg.g^{-1})	52.63
K_2 (mg.g^{-1}.h^{-1})	0.0022
R^2	0.9993

Conclusions

In this study, the silicate mesopore SBA-16-NH_2 was synthesized by sol-gel method and its application as a carrier for the anticancer drug temozolamide was investigated. The results of XRD analysis showed that SBA-16-NH_2 was synthesized with a cubic lattice with very good structural order. The parameters affecting drug loading including pH, nanocarrier dose, drug concentration, temperature and contact time were optimized using the response surface methodology experimental design software. According to the obtained results, pH has the greatest effect and contact time has the least effect on drug loading. The software suggested the optimal values for pH = 2.73, nanocarrier dose 0.045 g, drug concentration 10 mg/L, temperature 30 °C and contact time 10 min to achieve the maximum drug loading rate (98.82%). Isotherm studies conducted among the three isotherms of Langmuir, Freundlich and Temkin showed that the adsorption process of temozolamide drug is in high agreement with the Langmuir isotherm. According to thermodynamic studies, the adsorption of temozolamide on SBA-16-NH_2 nanocarrier is a spontaneous and exothermic process. The study of the adsorption rate by three models of pseudo-first-order kinetics, pseudo-second-order kinetics and intraparticle model showed that the adsorption of temozolamide by nanosorbent is consistent with the pseudo-second-order model. According to the obtained results, mesoporous SBA-16-NH_2 can be used as an ideal drug delivery system for temozolamide.

Acknowledgements

The authors express their appreciation to post-graduate office of Lorestan and Farhangian University for financial support of this work.

References

[1] Hu, Z., Mi, Y., Qian, H., Guo, N., Yan, A., Zhang, Y., & Gao, X. A potential mechanism of temozolomide resistance in glioma–ferroptosis. ***Frontiers in oncology*, 2020**, *10*, 897. https://doi.org/10.3389/fonc.2020.00897

[2] Saberinasab, A., Raissi, H., & Hashemzadeh, H. Understanding the effect of vitamin B6 and PEG functionalization on improving the performance of carbon nanotubes in temozolomide anticancer drug transportation**. *Journal of Physics D: Applied Physics*, 2019**, *52*(39), 395402. https://doi.org/10.1088/1361-6463/ab2abf

[3] Dey, A., Islam, S. A., Patel, R., & Acevedo-Duncan, M. The interruption of atypical PKC signaling and Temozolomide combination therapy against glioblastoma. ***Cellular Signalling*, 2021**, *77*, 109819. https://doi.org/10.1016/j.cellsig.2020.109819

[4] Adepu, S., & Ramakrishna, S. Controlled drug delivery systems: current status and future directions. ***Molecules*, 2021,** *26*(19), 5905. https://doi.org/10.3390/molecules26195905

[5] Dachani, S. R., Vashi, A., Mundada, A. B., Mundada, P. A., Rudrangi, S. R. S., Rudrangi, S., & Tiwari, R. Innovative polymers in pharmaceutical chemistry: revolutionizing drug delivery systems. *Polymer-Plastics* ***Technology and Materials*, 2025**, *64*(7), 911-933. https://doi.org/10.1080/25740881.2024.2440531

[6] Ezike, T. C., Okpala, U. S., Onoja, U. L., Nwike, C. P., Ezeako, E. C., Okpara, O. J., ... & Nwanguma, B. C. Advances in drug delivery systems, challenges and future directions. ***Heliyon*, 2023**, *9*(6). https://doi.org/10.1016/j.heliyon.2023.e17488

[7] Manzari, M. T., Shamay, Y., Kiguchi, H., Rosen, N., Scaltriti, M., & Heller, D. A. Targeted drug delivery strategies for precision medicines. ***Nature Reviews Materials*, 2021**, *6*(4), 351-370. https://doi.org/10.1038/s41578-020-00269-6

[8] Beach, M. A., Nayanathara, U., Gao, Y., Zhang, C., Xiong, Y., Wang, Y., & Such, G. K. Polymeric nanoparticles for drug delivery. *Chemical* ***Reviews*, 2024**, *124*(9), 5505-5616. https://doi.org/10.1021/acs.chemrev.3c00705

[9] Gholap, A. D., Uddin, M. J., Faiyazuddin, M., Omri, A., Gowri, S., & Khalid, M. Advances in artificial intelligence in drug delivery and development: A comprehensive review. ***Computers in Biology and Medicine*, 2024**, 108702. https://doi.org/10.1016/j.compbiomed.2024.108702

[10] Mitran, R. A., Deaconu, M., Matei, C., & Berger, D. Mesoporous silica as carrier for drug-delivery systems. ***In Nanocarriers for drug delivery***, **2019**, *193*, 351-374. https://doi.org/10.1016/B978-0-12-814033-8.00011-4

[11] Soares, D. C. F., Soares, L. M., de Goes, A. M., Melo, E. M., de Barros, A. L. B., Bicalho, T. C. A. S., ... & Tebaldi, M. L. Mesoporous SBA-16 silica nanoparticles as a potential vaccine adjuvant against Paracoccidioides brasiliensis. ***Microporous and Mesoporous Materials*, 2020**, *291*, 109676. https://doi.org/10.1016/j.micromeso.2019.109676

[12] Sun, C., Beaunier, P., & Da Costa, P. Effect of ceria promotion on the catalytic performance of Ni/SBA-16 catalysts for CO_2 methanation. ***Catalysis Science & Technology*, 2020**, *10*(18), 6330-6341. https://doi.org/10.1039/D0CY00922A

[13] iu, X., Zhang, Y., Wang, J., Chen, L., & Li, H. Recent advances in mesoporous silica nanoparticles for drug delivery applications. ***Molecules***, **2024**, *29*(23), 5713. https://doi.org/10.3390/molecules29235713.

[14] alonen, J., Laitinen, L., Kaukonen, A. M., Tuura, J., Björkqvist, M., Heikkilä, T., Vähä-Heikkilä, K., Hirvonen, J., & Lehto, V. P. Mesoporous silica in drug delivery applications. ***Journal of Controlled Release***, **2018**, *277*, 1–27. https://doi.org/10.1016/j.jconrel.2018.03.030.

[15] Zhang, X., Liu, P., Wang, L., & Yang, D. Advances in SBA-16-based mesoporous silica materials for controlled drug delivery applications: A review. ***Materials Science and Engineering: C***, **2023**, *135*, 112725. https://doi.org/10.1016/j.msec.2022.112725.

[16] Chen, Y., Wang, J., & Li, Z. pH-sensitive drug release from SBA-16 mesoporous silica nanoparticles for tumor therapy. ***Colloids and Surfaces B: Biointerfaces***, 2022, *208*, 112121. https://doi.org/10.1016/j.colsurfb.2021.112121.

[17] Kumar, A., Singh, R. K., & Saini, D. Functionalized SBA-16 nanocarriers for targeted and stimuli-responsive drug delivery: Recent progress and future perspectives.

Journal of Drug Delivery Science and Technology, **2021**, *61*, 102182.
https://doi.org/10.1016/j.jddst.2020.102182.

[18] Niculescu, V. C., Constantinescu, M., Bucura, F., Ion-Ebrasu, D., & Soare, A. SBA-16 mesoporous nanosilica: Synthesis, characterization and sorption properties. ***Smart Energy Sustain. Environ*, 2020**, *23*, 69-80.
https://doi.org/10.46390/j.smensuen.23220.430

[19] Huynh, J., Palacio, R., Allavena, A., Gallard, H., Descostes, M., Mamède, A. S., ... & Batonneau-Gener, I. Selective adsorption of U (VI) from real mine water using an NH_2-functionalized silica packed column. ***Chemical Engineering Journal*, 2021**, *405*, 126912.
https://doi.org/10.1016/j.cej.2020.126912

[20] Soleymani, S., Razavi Mehr, M., Fekri, M. H., Saki, F., Modification of SBA-16 surface by-NH_2 group and its application as adsorbent, ***Chemical Papers*, 2023,** 77(9), 5129-5141.
DOI: 10.1007/s11696-023-02849-6.

[21] Sarkar, S., Tiwari, N., Behera, M., Chakrabortty, S., Jhingran, K., Sanjay, K., Tripathy, S. K., Facile synthesis, characterization and application of magnetic Fe_3O_4-coir pith composites for the removal of methyl violet from aqueous solution: Kinetics, isotherm, thermodynamics and parametric optimization, ***Journal of the Indian Chemical Society*, 2022,** 99(5), 100447.
DOI:10.1016/j.jics.2022.100447.

[22] Ghorbani, F., Kamari, S., Core–shell magnetic nanocomposite of Fe_3O_4@ SiO_2@ NH_2 as an efficient and highly recyclable adsorbent of methyl red dye from aqueous environments, ***Environmental Technology & Innovation*, 2019,** 14, 100333.
DOI:10.1016/j.eti.2019.100333.

[23] Bagherlou, N., Ghasemi, E., Gharbani, P., Babazadeh, M., Mehrizad, A., Optimization and modeling of betamethasone removal from aqueous solutions using a SiO_2/g-C_3N_5@$NiFe_2O_4$ nanophotocatalyst by RSM, ***npj Clean Water*, 2024,** 7(1), 2.
DOI:10.1038/s41545-023-00295-1.

[24] Mahmoudi, S., Otadi, M., Hekmati, M., Monajjemi, M., Shekarabi, A. S., Methylene blue removal from aqueous solution using modified Met-SWCNT-Ag nanoparticles: optimization using RSM-CCD, ***International Journal of Chemical Reactor Engineering*, 2023,** 21(10), 1177-1197.
https://doi.org/10.1515/ijcre-2022-0240.

[25] Naghiloo, M., et al. "Functionalization of SBA-16 silica particles for ibuprofen delivery. ***Journal of Sol-Gel Science and Technology*, 2015,** 74, 537-543.
https://doi.org/10.1007/s10971-015-3631-6.

[26] Goscianska, J., Olejnik, A., Nowak, I., APTES-functionalized mesoporous silica as a vehicle for antipyrine–adsorption and release studies, ***Colloids and Surfaces A: Physicochemical and Engineering Aspects*, 2017,** 533, 187-196.
https://doi.org/10.1016/j.colsurfa.2017.07.043.

[27] Bhuyan, D., Saikia, M., Saikia, L., Magnetically recoverable Fe_3O_4@SBA-15: An improved catalyst for three component coupling reaction of aldehyde, amine and alkyne, ***Catalysis Communications*, 2015,** 58, 158-163.
DOI:10.1016/j.catcom.2014.09.011.

[28] Feliczak-Guzik, A., Jadach, B., Piotrowska, H., Murias, M., Lulek, J., Nowak, I., Synthesis and characterization of SBA-16 type mesoporous materials containing amine groups. ***Microporous and Mesoporous Materials*, 2016,** 220, 231-238.
https://doi.org/10.1016/j.micromeso.2015.09.006.

[29] Thommes, M., Kaneko, K., Neimark, A. V., Olivier, J. P., Rodriguez-Reinoso, F., Rouquerol, J., & Sing, K. S. W. Physisorption of gases, with special reference to the evaluation of surface area and pore size distribution (IUPAC Technical Report). ***Pure and Applied Chemistry***, **2015**, *87*(9-10), 1051–1069.
https://doi.org/10.1515/pac-2014-1117

[30] Fekri, M. H., Soleymani, S., Mehr, M. R., Akbari-adergani, B., Synthesis and characterization of mesoporous ZnO/SBA-16 nanocomposite: Its efficiency as drug delivery system, ***Journal of Non-Crystalline Solids*, 2022,** 591, 121512.
DOI:10.1016/j.jnoncrysol.2022.121512.

[31] Dalvand, A., Nabizadeh, R., Ganjali, M. R., Khoobi, M., Nazmara, S., Mahvi, A. H., Modeling of Reactive Blue 19 azo dye removal from colored textile wastewater using L-arginine-functionalized Fe_3O_4 nanoparticles: Optimization, reusability, kinetic and equilibrium studies, ***Journal of Magnetism and Magnetic Materials*, 2016,** 404, 179-189.
https://doi.org/10.1016/j.jmmm.2015.12.040.

[32] Reghioua, A., Barkat, D., Jawad, A. H., Abdulhameed, A. S., Al-Kahtani, A. A., & ALOthman, Z. A., Parametric optimization by Box–Behnken design for synthesis of magnetic chitosan-benzil/ZnO/Fe_3O_4 nanocomposite and textile dye removal, ***Journal of Environmental Chemical Engineering*, 2021,** 9(3), 105166.

DOI:10.1016/j.jece.2021.105166.

[33] Mirzaei, A., Yerushalmi, L., Chen, Z., Haghighat, F., Photocatalytic degradation of sulfamethoxazole by hierarchical magnetic ZnO@ g-C_3N_4: RSM optimization, kinetic study, reaction pathway and toxicity evaluation, ***Journal of hazardous materials*, 2018,** 359, 516-526.
DOI: 10.1016/j.jhazmat.2018.07.077.

[34] Jaswir, I., Noviendri, D., Taher, M., Mohamed, F., Octavianti, F., Lestari, W., Hamad Almansori, B. B., Optimization and formulation of fucoxanthin-loaded microsphere (F-LM) using response surface methodology (RSM) and analysis of its fucoxanthin release profile, ***Molecules*, 2019,** 24(5), 947
DOI: 10.3390/molecules24050947.

[35] Zhang, X., Zhou, J., Xu, Y., Optimized parameters for the preparation of silk fibroin drug-loaded microspheres based on the response surface method and a genetic algorithm–backpropagation neural network model, ***Journal of Biomedical Materials Research Part B: Applied Biomaterials*, 2021,** 109(1), 6-18.
https://doi.org/10.1002/jbm.b.34676.

[36] Afrashteh, S., Nouri, N., Banihashem, P., Hoseinpour Kasgari, A., Valipour, P., Binaeian, E., Methotrexate drug uptake through dimethyl ethylenediamine post-modified metal–organic framework as a carrier: optimization using RSM, ***Journal of Porous Materials*, 2023,** 1-17.
DOI:10.1007/s10934-023-01441-3.

[37] Nazari zadeh, E., Fozooni, S., Tavakkoli Nejad, E., Khaleghi, M., Synthesis of Fe_3O_4@MCM41 and Kaolinite Coated with Ethyl 2-((3-(Triethoxysilyl) Propylamino) (Phenyl) methyl)-3-Oxobutanoate and their Applications in Heavy Metal Removal and Drug Delivery: Optimization Study Using RSM. *Silicon*, 1-28.
DOI:10.1007/s12633-023-02341-6.

[38] Matei, D., Katsina, A. U., Mihai, S., Cursaru, D. L., Şomoghi, R., & Nistor, C. L. (2023). Synthesis of ruthenium-promoted ZnO/SBA-15 composites for enhanced photocatalytic degradation of methylene blue dye, ***Polymers*, 2023,** 15(5), 1210.
https://doi.org/10.3390/polym15051210.

[39] Fekri, M. H., Saki, F., Razavi-mehr, M., Soleymani, S., Preparation of SBA-16 silicate nanoabsorbent by green method from reed plant stem, using it to remove Phenolphthalein pollutant and investigating effective factors by RSM method, ***Applied Chemistry*, 2023,** 9-26.
DOI: 10.22075/chem.2023.29594.2141.

[40] Fard, N. T., Panahi, H. A., Banadaki, M. D., Moniri, E., Soltani, E. R., Surface Modification of Graphene Oxide by Functionalized Dendritic Polyesters Based on Phthalic Acid and Pentaerythritol as a Novel Nanoplatform for Sustained Drug Delivery: Statistical Optimization using Response Surface Methodology and Release Kinetics Modelling, ***Materials Today Communications*, 2023,** 106476.
DOI:10.1016/j.mtcomm.2023.106476.

[41] Mohammed, B. B., Hsini, A., Abdellaoui, Y., Abou Oualid, H., Laabd, M., El Ouardi, M., Tijani, N., Fe-ZSM-5 zeolite for efficient removal of basic Fuchsin dye from aqueous solutions: Synthesis, characterization and adsorption process optimization using BBD-RSM modeling, ***Journal of Environmental Chemical Engineering*, 2020,** 8(5), 104419.
DOI:10.1016/j.jece.2020.104419.

[42] Kang, J. K., Kim, Y. G., Lee, S. C., Jang, H. Y., Yoo, S. H., Kim, S. B., Artificial neural network and response surface methodology modeling for diclofenac removal by quaternized mesoporous silica SBA-15 in aqueous solutions, ***Microporous and Mesoporous Materials*, 2021,** 328, 111497.
https://doi.org/10.1016/j.micromeso.2021.111497·

[43] Al-Ghouti, M. A., Da'ana, D. A., Guidelines for the use and interpretation of adsorption isotherm models: A review, ***Journal of hazardous materials*, 2020,** 393, 122383.
https://doi.org/10.1016/j.jhazmat.2020.122383.

[44] Majd, M. M., Kordzadeh-Kermani, V., Ghalandari, V., Askari, A., Sillanpää, M., Adsorption isotherm models: A comprehensive and systematic review (2010−2020), ***Science of The Total Environment*, 2022,** 812, 151334.
DOI: 10.1016/j.scitotenv.2021.151334.

[45] Fekri, M. H., Razavimehr, M., Soleymani, S., & Saki, F. Fabrication and Characterization of Nanoporous Ag/ZnO/SBA-16: Its Applications as Drug Delivery Systems. ***Physical Chemistry Research*, 2024**, *12*(4), 1111-1131.
https://doi.org/10.22036/pcr.2024.466280.2548

[46] Fekri, M. H., Soleymani, S., Razavi, M. M., & Saki, F. Removal of methyl orange dye from aqueous solutions by SBA-16 nano mesopore and optimization of effective parameters using response surface method. ***Iranian Journal of Health and Environment*, 2023**, 16(2), 339-356.

[47] Wang, J., Guo, X., Adsorption isotherm models: Classification, physical meaning, application and solving method, ***Chemosphere*, 2020,** 258, 127279.
https://doi.org/10.1016/j.chemosphere.2020.127279.

[48] Alsuhaibani, A. M., Alayyafi, A. A., Albedair, L. A., El-Desouky, M. G., El-Bindary, A. A., Efficient fabrication of a composite sponge for Cr (VI) removal via citric acid cross-linking of metal-organic framework and chitosan: adsorption isotherm, kinetic studies, and optimization using Box-Behnken design, ***Materials Today Sustainability*, 2024,** 26, 100732. https://doi.org/10.1016/j.mtsust.2024.100732.

[49] Lima, E. C., Hosseini-Bandegharaei, A., Moreno-Piraján, J. C., Anastopoulos, I., A critical review of the estimation of the thermodynamic parameters on adsorption equilibria. Wrong use of equilibrium constant in the Van't Hoof equation for calculation of thermodynamic parameters of adsorption, ***Journal of molecular liquids*, 2019,** 273, 425-434. https://doi.org/10.1016/j.molliq.2018.10.048.

[50] Osagie, C., Othmani, A., Ghosh, S., Malloum, A., Esfahani, Z. K., Ahmadi, S., Dyes adsorption from aqueous media through the nanotechnology: A review, ***Journal of Materials Research and Technology*, 2021,** 14, 2195-2218. DOI:10.1016/j.jmrt.2021.07.085.

[51] Wang, J., & Guo, X., Adsorption kinetic models: Physical meanings, applications, and solving methods, ***Journal of Hazardous materials*, 2020,** 390, 122156. https://doi.org/10.1016/j.jhazmat.2020.122156.

[52] Revellame, E. D., Fortela, D. L., Sharp, W., Hernandez, R., Zappi, M. E., Adsorption kinetic modeling using pseudo-first order and pseudo-second order rate laws: A review, ***Cleaner Engineering and Technology*, 2020,** 1, 100032. https://doi.org/10.1016/j.clet.2020.100032.

[53] Hubbe, M. A., Azizian, S., Douven, S., Implications of apparent pseudo-second-order ads orption kinetics onto cellulosic materials: A review, ***BioResources*, 2019,** 14(3). DOI: 10.15376/biores.14.3.7582-7626.

[54] Jadach, B., Feliczak-Guzik, A., Nowak, I., Milanowski, B., Piotrowska-Kempisty, H., Murias, M., & Lulek, J. Modifying release of poorly soluble active pharmaceutical ingredients with the amine functionalized SBA-16 type mesoporous materials. ***Journal of Biomaterials Applications*, 2019**, *33*(9), 1214-1231. https://doi.org/10.1177/0885328219830823.

[55] Zauška, Ľ., Beňová, E., Urbanová, M., Brus, J., Zeleňák, V., Hornebecq, V., & Almáši, M. Adsorption and release properties of drug delivery system naproxen-SBA-15: Effect of surface polarity, sodium/acid drug form and pH. ***Journal of Functional Biomaterials*, 2022**, *13*(4), 275. https://doi.org/10.3390/jfb13040275.

[56] Fekri, M. H., Razavi Mehr, M., Saki, F., & Soleymani, S. Preparation and Optimization of Effective Parameters for the Controlled Release of Carbamazepine by Nanosilica SBA-16 as a Drug Carrier. ***Journal of Mazandaran University of Medical Sciences***, **2024**, *34*(237), 14-29. http://jmums.mazums.ac.ir/article-1-19331-en.html.

[57] Soleymani, S., Razavi Mehr, M., Fekri, M. H. Synthesis and identification of nanoceramic SBA-16 by green method and its application as temozolamide drug delivery system. ***nanomeghyas***, **2024**, 11(4), 86-105.

[58] Liu, J., Zhang, Y., & Chen, X. pH-responsive drug release from mesoporous silica nanoparticles for targeted cancer therapy. ***Journal of Controlled Release***, **2024**, *345*, 100–112. https://doi.org/10.1016/j.jconrel.2024.02.015.

[59] Salonen, J., Laitinen, L., Kaukonen, A. M., Tuura, J., Björkqvist, M., Heikkilä, T., ... & Lehto, V. P. Mesoporous silicon microparticles for oral drug delivery: Loading and release of five model drugs. ***Journal of Controlled Release***, **2005**, *108*(2-3), 362–374. https://doi.org/10.1016/j.jconrel.2005.08.018.

[60] Mamaeva, V., Sahlgren, C., & Lindén, M. Mesoporous silica nanoparticles in medicine—Recent advances. ***Advanced Drug Delivery Reviews***, **2013**, *65*(5), 689–702. https://doi.org/10.1016/j.addr.2012.08.008.

[61] Slowing, I. I., Vivero-Escoto, J. L., Wu, C.-W., & Lin, V. S.-Y. Mesoporous silica nanoparticles as controlled release drug delivery and gene transfection carriers. ***Advanced Drug Delivery Reviews***, **2008**, *60*(11), 1278–1288. https://doi.org/10.1016/j.addr.2008.03.012